

Electronic structure studies of Ni–X (X: B, S, P) alloys using x-ray photoelectron spectroscopy, x-ray induced Auger electron spectroscopy and density functional theory calculations

This article has been downloaded from IOPscience. Please scroll down to see the full text article.

2009 J. Phys.: Condens. Matter 21 245503

(<http://iopscience.iop.org/0953-8984/21/24/245503>)

View [the table of contents for this issue](#), or go to the [journal homepage](#) for more

Download details:

IP Address: 129.252.86.83

The article was downloaded on 29/05/2010 at 20:11

Please note that [terms and conditions apply](#).

# Electronic structure studies of Ni–X (X: B, S, P) alloys using x-ray photoelectron spectroscopy, x-ray induced Auger electron spectroscopy and density functional theory calculations

S Diplas<sup>1</sup> and O M Løvvik

SINTEF Materials and Chemistry, Forskningsv n 1, NO-0314 Oslo, Norway

and

Department of Physics, University of Oslo, Box 1048 Blindern, NO-0316 Oslo, Norway

E-mail: [Spyros.Diplas@sintef.no](mailto:Spyros.Diplas@sintef.no)

Received 10 March 2009, in final form 28 April 2009

Published 21 May 2009

Online at [stacks.iop.org/JPhysCM/21/245503](http://stacks.iop.org/JPhysCM/21/245503)

## Abstract

The electronic structure of Ni–X (X = B, S, P) alloys was studied using x-ray photoelectron spectroscopy, x-ray induced Auger electron spectroscopy and density functional theory. The spectroscopic data in the form of the Ni 2p shake-up satellite and the Ni 2p LMM, P 2p KLL and S 2p KLL Auger parameters combined with density of states (DOS) and charge difference plots suggest an overall charge transfer from the Ni sites towards the alloying addition sites. However, this is masked, with intra-atomic charge redistribution leading to an increased occupancy of the Ni 3d states in the alloys. The Ni 3d DOS shows strong similarity to that of Pt which is the best catalyst for hydrogen evolution.

(Some figures in this article are in colour only in the electronic version)

## 1. Introduction

Nickel is a promising catalyst for hydrogen production by water electrolysis but its high overpotential prohibits its use as an electrode. It was shown that alloying Ni with B, S and P reduces the overpotential and increases the catalytic activity by three orders of magnitude as compared to that of pure Ni [1–3]. In a previous paper we have addressed the reasonable scepticism as to whether the catalytic activity takes place on the ‘metallic’ surface of the Ni alloy or on an oxide, formed by exposure to either the aqueous electrolyte or in air during handling of the samples or both [4]. It was argued that it is the absence of long range order and the amorphous/nanocrystalline nature of the alloy itself that governs the catalytic properties. The electrochemical removal of the oxides present on the alloy surface enhances the catalytic properties of the alloys,

indicating that the oxide(s) inhibit rather than catalyzing the hydrogen evolution reaction ([4] and references 1, 3, 4 therein).

Since the electronic properties of the alloy surfaces play an important role in the catalytic activity, investigations of the changes in Ni electronic structure happening upon alloying with B, S and P are important for a better understanding of the improved catalytic behaviour. Previous research on Ni catalytic alloys [5–9] utilized arguments involving charge transfer between Ni and P, S, and B atoms. These arguments were based on x-ray photoelectron spectroscopy (XPS) results such as measured core level energy shifts between elements in elemental and alloying states. The measurable chemical shift is one of the main advantages of using XPS as an analytical technique. The chemical shift is defined as the variation in the measured photoelectron (and/or Auger electron) energy arising from changes in the atomic potential, which are in turn strongly related to changes in the atomic environment. Photoelectron binding energy values are susceptible to energy referencing

<sup>1</sup> Address for correspondence: SINTEF Materials and Chemistry, Forskningsv n 1, NO-0314 Oslo, Norway.

and/or sample electrostatic charging effects. These effects can be minimized by e.g. measuring peak energy differences (shifts) in the same spectrum and using the same spectrometer to analyse materials under the same conditions. In peak shifts of elements in non-conducting samples we assume negligible changes in the sample work function. In addition, peak shifts contain contributions from both initial and final state effects (see equation (1) in section 3.2). The use of the Auger parameter (AP), defined as the sum of the binding energy of the photoelectron and the kinetic energy of the associated Auger electron (see equation (2) in section 3.2 below), not only neutralizes energy referencing but further provides a means of separating final and initial state effects (see equations (2) and (3)).

A pictorial description of the AP dependence on chemical state variations is given by the chemical state or Wagner plots [10, 11]. In such a plot the binding energy of a peak (i)  $E_{B(i)}$  is plotted against the kinetic energy of the equivalent Auger peak (ijj) ( $E_{K(ijj)}$ ) (see figures 3–5 in section 3.2). The Auger kinetic energy values lie on the ordinate and the photoelectron binding energy values on the abscissa oriented in the negative direction. The Auger parameters are then expressed in terms of the linear relationship of the Auger peak versus the photoemission peak and lie on the straight lines with slope +1 (final state) and +3 (initial state) [11]. This means that all points lying on each line correspond to the same Auger parameter value.

In addition to absolute and relative shifts of the primary spectral structure, expressed as changes in the photoelectron binding energy and the AP respectively, secondary spectral features (e.g. energy loss features attributed to plasmon peaks and shake-up satellites) can be used for electronic structure studies. There is an extensive literature devoted to the interpretation of the Ni 2p satellite and its variation in different chemical environments. The presence of the Ni 2p satellite can be summarized using the Kotani–Toyoizawa model [12]. Above photoemission the presence of the core hole drags the Ni d level, which in the initial state is above the Fermi level ( $E_F$ ), to lower energies below  $E_F$ . Therefore, in the final state the Ni d level can in principle accommodate additional electrons through screening processes. The Ni 2p satellite is related to electron screening within the Ni 4s band instead of the d band leading to a two-hole state ( $3d^94s^2$ ) whilst the main Ni 2p line is associated with 3d screening. The satellite intensity seems to depend on the weight of unoccupied 3d states and its position above  $E_F$  [13]. Upon alloying Ni with electronegative elements the satellite intensity was seen to increase [13]. The opposite trend was seen upon alloying with electropositive elements. This satellite behaviour was generally interpreted as charge transfer from (increased satellite intensity) and towards (reduced satellite intensity) the Ni sites respectively [13]. It should be noted here that according to the Kotani–Toyoizawa model the term ‘shake-up satellite’ is not very appropriate since its interpretation implies screening rather than ‘shake-up’ events. We chose therefore to use the general term ‘2p satellite’ rather than ‘shake-up satellite’ when referring to this secondary spectral feature.

In previous studies, we have used XPS data, in the form of the Ni 2p satellite and the Ni AP, to probe electronic structure

variations in Ni–B, Ni–S and Ni–P alloys [4, 14]. In this paper we use DFT calculations on the Ni–B, Ni–P, Ni–S systems and XPS and XAES data in the form of Ni, P and S Auger parameters (AP) in an effort to probe the electronic changes occurring upon alloying of Ni with B, S and P. We compare this data with our previous XPS studies of changes in the Ni 2p satellite energy and intensity and variations in the Ni 2p LMM AP in Ni–X (X = B, S, P) alloys [4, 14] in order to facilitate subsequent discussions. We also attempt, through atomistic modelling, to obtain a better insight into the spectroscopic observations such as changes in Ni 2p satellite intensity and energy as well as variations in the Ni, P and S AP.

## 2. Materials and methods

The Ni–B, S and P alloys studied were produced with electrodeposition and the processing details are included in previous papers [1–4, 14]. XPS and XAES were performed using a VG Scientific ESCALAB Mk II fitted with a Thermo Electron Corporation Alpha 110 hemispherical analyser and Mg  $K\alpha$  radiation ( $h\nu = 1253.6$  eV). Survey and high resolution spectra were acquired at pass energies of 100 and 20 eV respectively. The use of the continuous Bremsstrahlung radiation generated by the 12 keV electrons entering the target enabled excitation of P and S 1s electrons with accompanying emission of P and S KLL Auger electrons respectively [15, 16]. The surface of the sample was analysed after short periods of Ar ion etching (4 keV) until the C 1s and O 1s signals were minimized. By monitoring the Ni, P, S 2p and B 1s as well as the C and O 1s peaks in between the etching intervals we were confident that etching did not affect the sample stoichiometry; it only diminished surface contamination. Data processing was performed using the CasaXPS software [17].

Calculations were performed within density functional theory (DFT) using the PW91 generalized gradient approximation (GGA) [18]. The calculations were performed using the Vienna *ab initio* simulation package (VASP) [19, 20], which employs plane waves as basis functions. The projector augmented wave (PAW) method [21] was used to represent the electron density; this is a generalization of the linearized augmented plane wave (LAPW) and the pseudopotential (PP) methods, with reliability comparable to that of LAPW methods and efficiency close to that of PP methods [21]. The density of  $\mathbf{k}$  points in the reciprocal space integration was always kept below  $0.2 \text{ \AA}^{-1}$ . The tetrahedron method with Blöchl corrections was used to smear partial occupancies near the Fermi level. The criterion for self-consistency was a change in total electronic energy of less than  $10^{-5}$  eV between two electron density iterations. The cut-off energy for the plane wave expansion was 500 eV. A quasi-Newton formalism was used to minimize the crystal structures, and the unit cell size and shape were allowed to relax simultaneously with the atomic positions for all the structures. The convergence criterion for the structural optimization was the forces being less than  $0.05 \text{ eV \AA}^{-1}$ .

Since the calculations are periodic, we are restricted to crystalline models of the Ni compounds. This is a tough restriction, particularly since the Ni alloys studied with XPS/XAES were amorphous/nanocrystalline and also some

of the stoichiometries that we are aiming at do not exist as crystalline compounds. The compositions of the alloys studied are Ni–50 at.% B, Ni–22% S, and Ni–30% P; at these compositions the materials exhibit the maximal catalytic activity [1–4, 14]. The first composition can easily be represented by the NiB compound, whose crystal structure is within the  $Cmcm$  space group [22], and Ni<sub>2</sub>P (space group  $P6\bar{2}m$  [23]) represents the Ni–30% P compound fairly well. For the Ni–22% S compound, however, there are no crystalline Ni–S compounds resembling the stoichiometry; the Ni–S compound with the lowest S content known is Ni<sub>3</sub>S<sub>2</sub> (40% S). One alternative could be to use the Ni<sub>3</sub>B or Ni<sub>3</sub>P compounds identified as model structures for a hypothetical Ni<sub>3</sub>S structure. However, since Pd<sub>3</sub>B has the same crystal structure as Ni<sub>3</sub>B (space group  $Pnma$  [24]), we have chosen to use Pd<sub>3</sub>S (space group  $Ama_2$  [25]) as the model structure for Ni<sub>3</sub>S.

### 3. Results and discussion

#### 3.1. Ni–B, P, S solid solubility

The thermodynamic equilibria of Ni with P, S and B in the compositional ranges studied in this work are characterized by limited or negligible solid solubility [26]. This is partly due to the large difference in nominal atomic size between Ni and the alloying additions, and the different crystal structures and valencies. Although the above differences may explain the absence of solid solubility, the small difference in (Pauling) electronegativity between Ni and B, P and S [27]—0.1, 0.3 and 0.6 respectively (B, P and S being more electronegative)—cannot really clarify the presence of a series of line compounds in the binary phase diagrams. Thus, the traditional criteria for substitutional solid solubility such as the Hume-Rothery empirical rules [28] are rather inadequate for explaining the alloying behaviour of Ni with B, S and P.

#### 3.2. Electron screening and the use of the Auger parameter

Changes in the atomic environment are detectable with XPS via energy shifts ( $\Delta E_i$ ) of the photoelectron peaks in the XPS spectrum:

$$\Delta E_{(i)} = k\Delta q + \Delta V_M - \Delta R \quad (1)$$

where  $\Delta E_{(i)}$  is the shift of the binding energy of the photoelectron ejected from level  $i$ ,  $\Delta q$  is the contribution of the changes in valence charge,  $\Delta V_M$  describes the contribution from the Coulomb interaction between the photoelectron ( $i$ ) and the surrounding charged atoms and  $\Delta R$  is the final state contribution expressed as the relaxation energy change arising from the response of the local electronic structure to the screening of the core hole. In equation (1), differences in sample work function, for insulators, are considered negligible. From (1) it is therefore evident that  $\Delta E_{(i)}$  contains initial state contributions (first and second term) as well as final state contributions expressed via the third term  $\Delta R$ . The higher the screening efficiency of the surrounding electrons is, the larger the relaxation energy becomes. The screening efficiency of a system in the presence of core holes is better described by the final state Auger parameter (see e.g. [29]) as defined by

Gaarenstroom and Winograd [30] using the sum of the binding energy of the photoelectron emitted from level  $i$  ( $E_{Bi}$ ) and the kinetic energy of the equivalent Auger electron ( $E_{Kij}$ ):

$$\alpha' = BE_i + KE_{ij}. \quad (2)$$

Initial state effects are described by the initial state AP [31] given by formula (3)

$$\beta = KE_{(ij)} + BE_{(i)} + 2BE_{(j)}. \quad (3)$$

By assuming all core level shifts between two different environments to be the same, it can be shown that the changes in the final state Auger parameter  $\Delta\alpha'$  are equal to twice the change in polarization energy ( $\Delta R$ ) (see equation (4)):

$$\Delta\alpha' = 2\Delta R. \quad (4)$$

The changes in the polarization energy arise from alterations in the intra-atomic (final state valence electrons) and extra-atomic environment (see e.g. [11]). However, in the case of transition elements,  $\Delta\alpha'$  and  $\Delta R$  are not directly linked as described above due to complications arising from d–s interband charge transfer [32]. Changes in the initial state AP ( $\Delta\beta$ ) reflect changes in the atomic potential according to equation (5) [31]:

$$\Delta\beta = 2\Delta V. \quad (5)$$

By using the different forms of the AP as described above, we can separate final and initial state effects coexisting in the definition of the binding energy in equation (1).

Figure 1 shows the main features of the high resolution spectra used in the analysis. Figures 2 and 3 show the relative positions of the P and S 1s KLL Auger parameters with respect to pure P and S as well as other P- and S-containing compounds, and figures 4–6 show chemical state plots for P (figure 4), S (figure 5) and Ni (figure 6). According to the definition of  $\alpha'$  and  $\beta$  in equations (2) and (3), two sets of lines are drawn with slopes +1 and +3 representing compounds having the same final state (line with slope +1) and initial state (line with slope +3) Auger parameter. The comparison of equations (2) and (3) with the lines in figures 4–6 shows that the final and initial state AP are the intercepts on the ordinate, whilst the slopes correspond to the double and triple weighing of the binding energy in the definition of  $\alpha'$  and  $\beta$  respectively. In the sections below we comment on the initial and final state Auger parameters of Ni, P and S in the context of equations (4) and (5), and the chemical state plots in figures 4–6. Since the Auger parameter analysis requires well localized core–core–core (C–C–C) Auger transitions in figure 6 we use the C–C–C Ni LM<sub>23</sub>M<sub>23</sub> Auger line (see figure 1(f)), instead of the more intense Ni 2p LM<sub>45</sub>M<sub>45</sub> (see figure 1(e)) which nevertheless involves the valence band. Auger parameter changes in transition metals are in general small. This has been attributed to the occurrence of a local screening mechanism [11], which involves movement of the screening electron from the relatively narrow valence band of the transition metal to the localized atomic orbital of the core-ionized atom. Thus, the AP of the transition metal is relatively insensitive to the chemical environment due to overshadowing

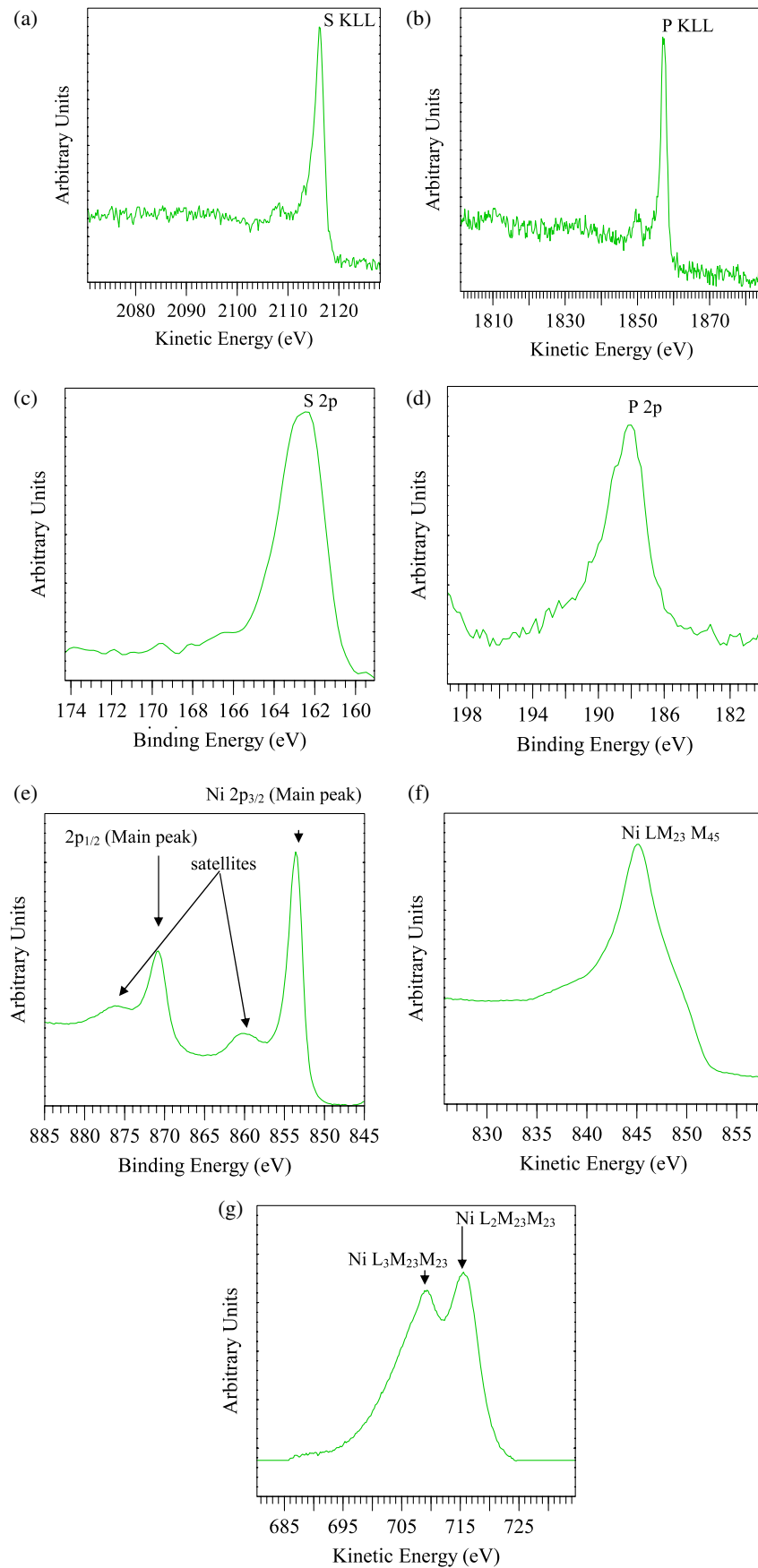


**Figure 1.** High resolution spectra used in the analysis: (a) Bremsstrahlung induced S KLL, (b) Bremsstrahlung induced P KLL, (c) S 2p, (d) P 2p, (e) Ni 2p spectra showing the main peaks and the satellites, (f) Ni LM<sub>23</sub>M<sub>45</sub> Auger peak, (g) Ni LM<sub>23</sub>M<sub>23</sub> Auger peaks.

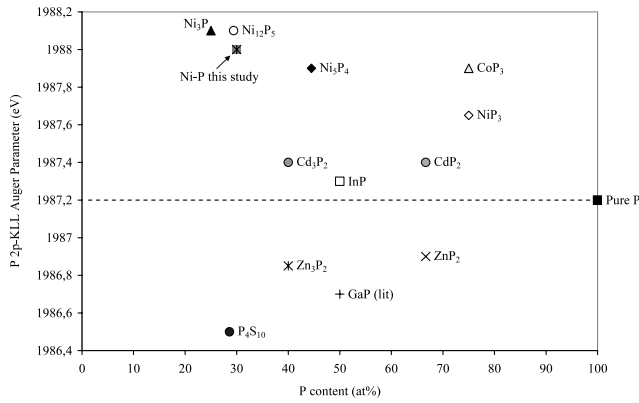


**Figure 2.** P 2p KLL Auger parameter values of several P-containing compounds. The AP of the Ni–P alloy in this study is positioned well above that of pure P.

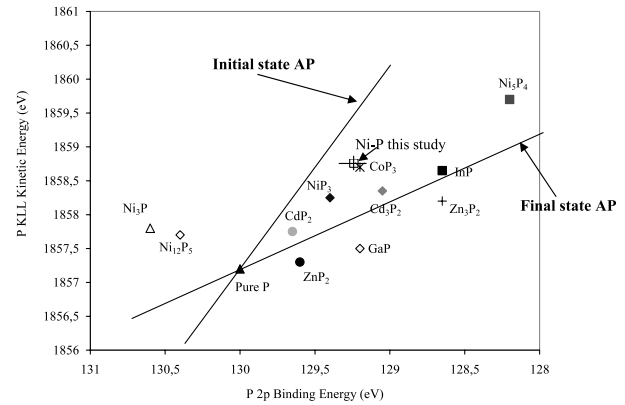


**Figure 4.** P 2p KLL chemical state plot of P-containing compounds. The Ni–P alloy in this study shows a higher final state Auger parameter and a lower initial state Auger parameter than pure P.

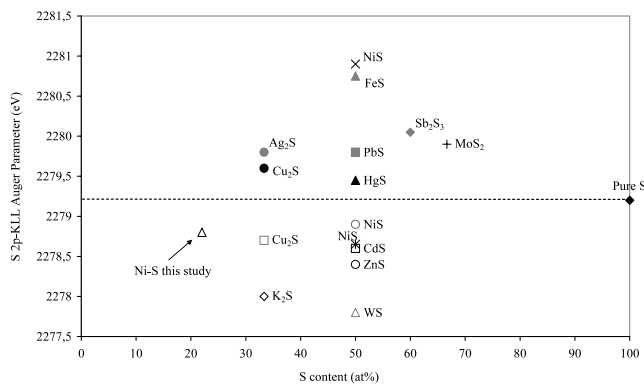


**Figure 3.** S 2p KLL Auger parameter values of several S-containing compounds. The AP value of the Ni–S alloy in this study is positioned below that of pure S.

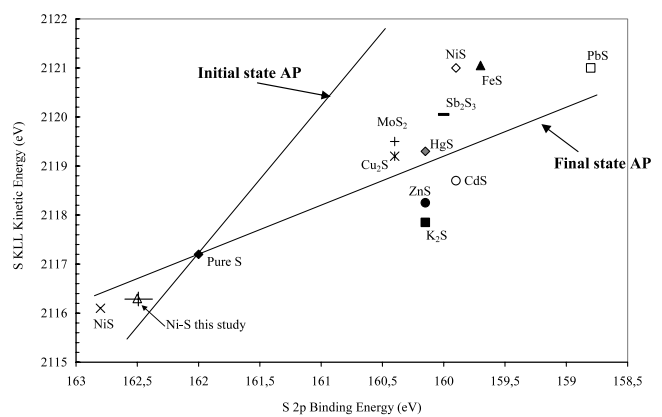


**Figure 5.** S 2p KLL chemical state plot of S-containing compounds. The Ni–S alloy in this study shows a lower final state Auger parameter and a higher initial state Auger parameter than pure S.

by the large atomic relaxation energy involved in the electron transfer of the above local screening mechanism [11]. The changes in Ni AP in the present work, although small and just outside the experimental error, show a trend and are therefore included in the subsequent discussion.

**3.2.1. Ni–P alloys.** Figures 2 and 4 show that the  $\alpha'$  values for P in the Ni–P alloys lie higher than those for pure P, indicating thus that the core holes on the P atoms are better screened in the alloy atomic environment than in the elemental P atomic environment. The lower  $\beta$  values for P in the Ni–P alloys (figure 4) indicate that the core holes experience a more negative atomic potential as compared to the elemental P case. The changes in  $\alpha$  and  $\beta$  may be interrelated since an increased screening of the core holes could be a result of increased ‘on site’ electron density due to inter-atomic charge transfer. Charge transfer from Ni sites towards the P sites, expected from an electronegativity point of view, could therefore explain the changes in P AP and also the reduced  $\alpha$  values for Ni in the Ni–P alloys as compared to pure Ni. A reduced electron density around the Ni atoms could be reflected in a reduced core hole screening efficiency (i.e.  $\Delta R < 0$  and therefore  $\Delta\alpha' < 0$ ). However, a reduced electron density around the Ni sites would reasonably cause a positive change in the atomic

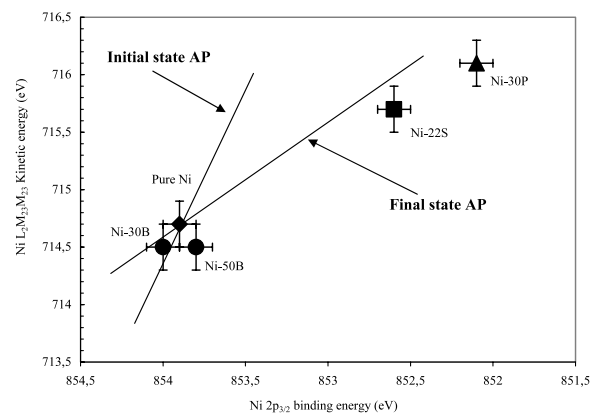


**Figure 6.** Ni 2p  $L_2M_{23}M_{23}$  chemical state plots of Ni–X (X = B, S, P) alloys. The Ni alloys appear to have lower final and initial state Auger parameters as compared to pure Ni.

potential and therefore according to (5)  $\Delta\beta > 0$ . Similarly, according to the analysis in section 1, the Ni 2p satellite intensity should increase [12, 13]. From figures 6 and 7 this is not the case and more complicated charge transfer phenomena take place, as shown by the DFT results in section 3.3.

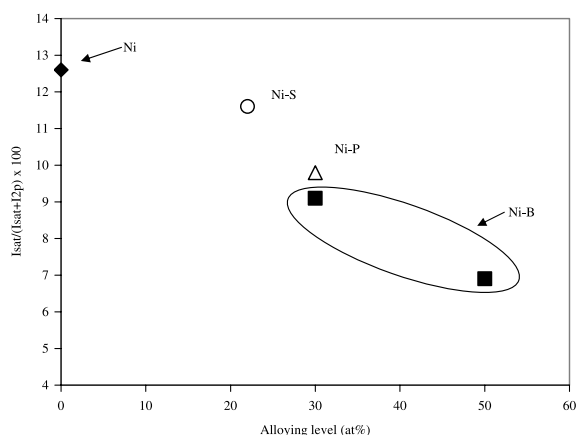


**Figure 7.** Variation of the Ni 2p satellite upon alloying with S, P and B. The difference in satellite intensity increases in the order Ni–S, Ni–P, Ni–B. This is in agreement with the displacement of the Ni 3d band from the Fermi level in figure 9 which is higher for Ni–B and lower for the Ni–S alloy.

**3.2.2. Ni–S alloys.** As shown by figures 3 and 5 the  $\alpha'$  value for S in the Ni–S alloy lies lower than that for pure S, indicating an inferior electron screening of the S core holes in the alloy as compared to the case for elemental S. The higher  $\beta$  values for S in the Ni–S alloys indicate that the core holes experience a less negative atomic potential as compared to the case for elemental S. This behaviour can again be explained in terms of an S to Ni electron transfer, which contradicts however the electronegativities of the two elements. A simple charge transfer (from S to Ni) argument can also explain the lower  $\beta$  values for Ni in the Ni–S as well as the reduction in the Ni 2p satellite intensity (figure 7). It cannot however clarify the lower  $\alpha'$  values for Ni in the Ni–S alloys in the framework of a reduced screening due to reduced on site electron density argumentation. Again a simplified inter-atomic charge transfer picture is not conclusive.

**3.2.3. Ni–B alloys.** For Ni–B alloys we have AP data only for Ni. Auger parameter data for B are not provided due to the lack of a sharp core–core–core (CCC) B Auger peak. As shown in figure 6 the  $\alpha$  values for Ni in the Ni–B alloys lie lower than that for pure Ni, indicating an inferior electron screening of the Ni core holes in the alloys as compared to elemental Ni. Ni also acquires lower (Ni–50 at.% B) or similar (Ni–30 at.% B)  $\beta$  values in the alloyed state as compared to the

elemental state. Again a simple electron transfer from Ni to B is in accordance with the electronegativity expectations and would explain the reduced screening of the Ni core holes in the alloy environment. However, the negative  $\Delta\beta$  values and the reduction in the Ni 2p satellite intensity (figure 7) cannot be explained by a simplified Ni to B charge transfer since they may well assume an increased electron density on the Ni atoms in the Ni–B alloys.

### 3.3. Density of states, intra-atomic charge transfer and inter-atomic charge distribution

It is apparent from the above analysis that it is difficult to draw clear conclusions from the experimental results alone. We have therefore complemented the experiments by performing first-principles calculations based on density functional theory. This will add detail to the characterization, and may assist in removing any ambiguities remaining from the experiments. Such charge analyses can be executed as either space-resolved or state-resolved ones; performing both types can contribute considerably to complementing the spectroscopic data above.

If we first look at the charge transfer plots in figure 8, it is evident that there is generally a charge transfer from Ni to the additives. This is expected, considering the electronegativities of the elements. In the case of the B-containing alloys, the largest gain in charge is between the B atoms, indicating a covalent type bond between neighbour B atoms. On the other hand, both P and S gain charge significantly in the near-core region. (The core regions should not be considered for any of the atoms, since only valence electrons are fitted by VASP.)

The calculated electronic density of states (DOS) may further assist in the interpretation of the experimental spectra. It is instructive to see first how the amount of additive to Ni contributes to the DOS. We have plotted the total and projected DOS of Ni with different B contents in figure 9, and see that there are some clear trends when moving from pure Ni to NiB. First of all, the total DOS exhibits two main peaks in the valence band which move to a lower energy relative to the Fermi level as the B content increases. Thus, the peak which is located at the Fermi level for pure Ni has moved to  $-1.9$  eV for NiB. Similarly, the second-highest peak in Ni at  $-1.6$  eV moves down to  $-3.7$  eV for NiB. From the projected DOS we see that this is primarily due to the Ni d states, which move down as B is added. It is interesting to compare the above picture with Pt, which is the best element known for hydrogen catalysis [33]. Pt has three large peaks in the total DOS,

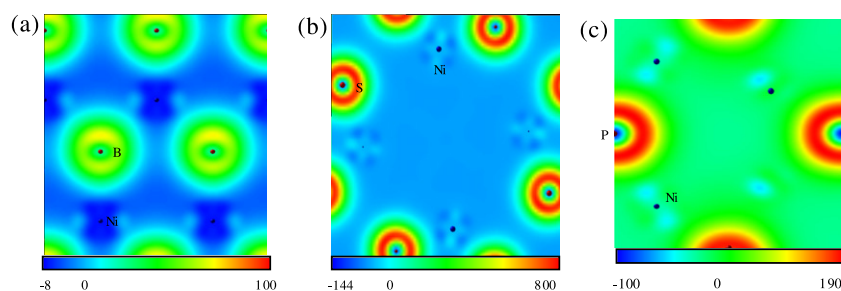


**Figure 8.** Charge difference plots for the NiB (a), Ni<sub>3</sub>S (b) and Ni<sub>2</sub>P (c) compounds.

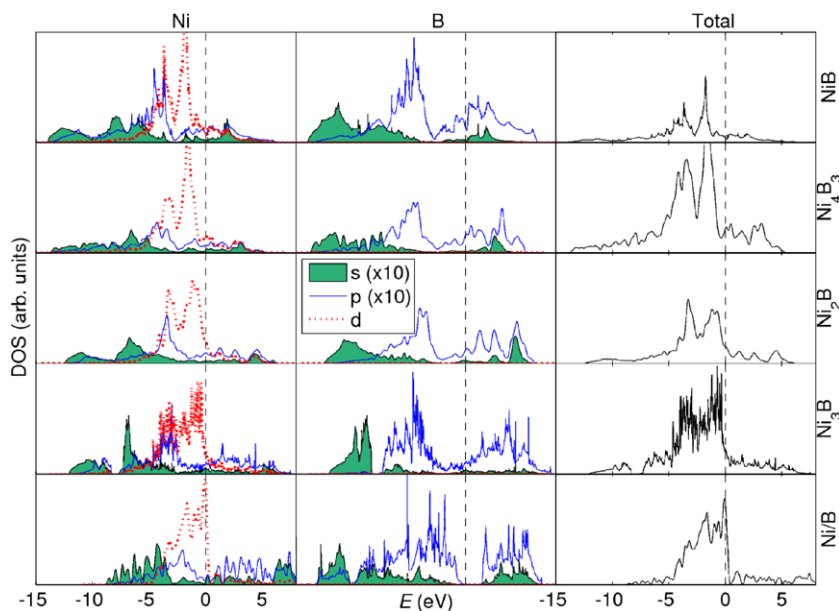


**Figure 9.** Partial and total electronic densities of states (DOS) for Ni compounds with increasing B content; from the lower panel they include pure Ni, Ni–25 at.% B ( $\text{Ni}_3\text{B}$ ), Ni–33 at.% B ( $\text{Ni}_2\text{B}$ ), Ni–43 at.% B ( $\text{Ni}_4\text{B}_3$ ), and Ni–50 at.% B ( $\text{NiB}$ ). Pure B is shown in the bottom centre panel, while the bottom right panel is the total DOS of pure Ni. Green filled, blue solid and red dotted curves represent s, p, and d electrons, respectively (s and p densities are multiplied by 10 for the sake of comparison). Energies are measured in eV relative to the Fermi level.

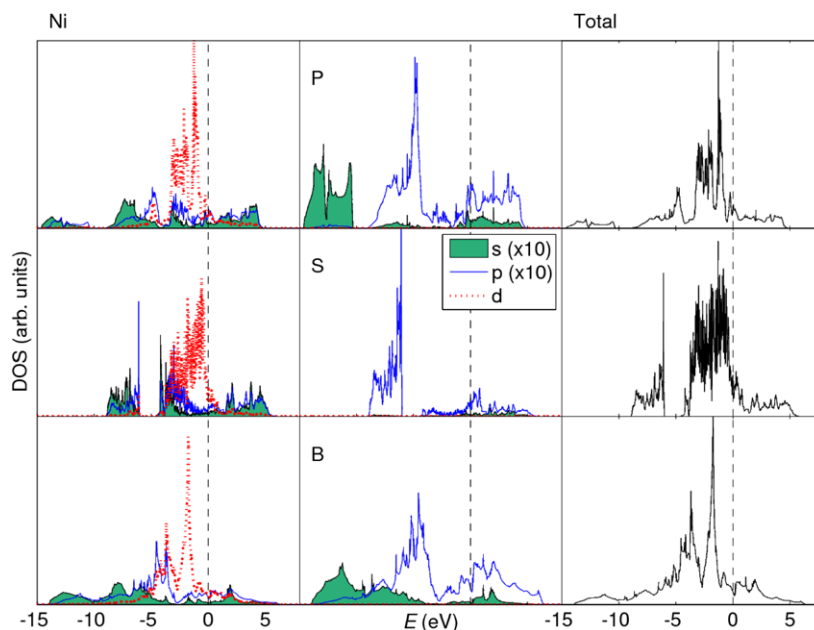


**Figure 10.** Total and projected DOS for  $\text{NiB}$  (bottom),  $\text{Ni}_3\text{S}$  (middle) and  $\text{Ni}_2\text{P}$  (top). Green filled, blue solid and red dotted curves correspond to s, p, and d electrons, respectively (s and p densities are multiplied by 10 for the sake of comparison). Energies are measured in eV relative to the Fermi level.

corresponding to peaks in the d states, at 0,  $-1.9$ , and  $-3.4$  eV. The two latter are at almost exactly the same position as the two peaks for  $\text{NiB}$ , which confirms that there is a connection between the location of d peaks and the catalytic activity of a material. This is even more striking when we compare in addition the calculated DOS for  $\text{Ni}_2\text{P}$  and  $\text{Ni}_3\text{S}$  in figure 10. It turns out that all these compounds have at least two major peaks in the Ni d states in the same area below the Fermi level. Although the catalytic activity of the Ni alloys in the present

study refers to hydrogen evolution, it should be nevertheless noticed that the above picture is consistent with the common notion that the d band position is important for hydrogenation catalysis [33].

#### 3.4. Discussion

The charge difference plots for the  $\text{NiB}$ ,  $\text{Ni}_3\text{S}$  and  $\text{Ni}_2\text{P}$  compounds, shown in figure 8, show that the general charge



transfer direction is from Ni towards the alloying addition. For the Ni–B alloys the inter-atomic bonding has a strongly covalent character. In addition to the overall charge transfer indicated by the charge difference plots, the projected DOS in figures 9 and 10 indicate that the Ni 3d levels are more occupied in the alloys than in pure Ni, since parts of the d band move from the conduction band to occupied states in the valence band. The overall Ni  $\rightarrow$  X (X = B, S, P) charge transfer is responsible for the overall reduced screening efficiency of the core holes in Ni as reflected in the Ni final state Auger parameter  $\alpha'$ . The shift of the potential to more negative values for the alloys compared to pure Ni as expressed by the initial state Auger parameter  $\beta$  could be explained by the increase in the d population of Ni in the alloys.

There is most probably an increase in the Ni 3d population in the Ni–X alloys because of the shift of the Ni 3d band away from  $E_F$ . Since this is accompanied with a net loss of charge from Ni, it means that there must be inter-atomic charge redistribution towards 3d in Ni. The shift of the Ni 3d band increases in the order Ni–B > Ni–P > Ni–S (see figure 10), in agreement with the order of the reduction in 2p satellite intensity (see figure 7). As mentioned in section 1, the main Ni 2p peak and the associated satellite correspond to two distinct final states after the photoemission, namely the  $c^{-1}3d^{10}4s$  and the  $c^{-1}3d^94s^2$  respectively. A reduction in the satellite intensity compared to the main peak signifies that the final state  $c^{-1}3d^{10}4s$  is more probable, which is consistent with an increased Ni 3d population when moving from Ni–S to Ni–P and Ni–B.

The satellite—main line separation reflects the difference of the relaxation energies associated with the two states. Our *ab initio* calculations show an initial state shift of the Ni 3d state in the alloys below the  $E_F$ . There are therefore fewer Ni 3d unoccupied states in the alloys than in the pure Ni state. According to the Kotani–Toyozawa model [12] it is therefore less likely for the unoccupied Ni 3d levels to be dragged below  $E_F$  upon photoemission since their number is decreased in the initial state. As a result, the well screened  $c^{-1}3d^{10}4s$  final state associated with the main peak will dominate over the  $c^{-1}3d^94s^1$  state associated with the satellite. The Ni 2p satellite energy was also seen to increase in the order Ni–B > Ni–P > Ni–S [4] denoting thus an increasingly superior relaxation associated with the main peak in the same order. The increased 3d band occupancy may also explain the reduced Ni final state AP in the alloys since the extra-atomic screening of the core hole via extra-atomic charge transfer to the Ni 3d band is expected to be reduced in the alloys.

As far as the alloying additions are concerned, the changes in initial and final state APs are explained by the overall charge transfer but also by the on site (intra-atomic) charge decomposition. The Ni to P overall charge transfer implies increased screening conditions for the P core holes in the Ni–P alloy (increased  $\alpha'$ ) and a more negative Madelung potential (reduced  $\beta$ ). The overall Ni  $\rightarrow$  S charge transfer can explain neither the reduced  $\alpha$  value nor the increased  $\beta$  value for S in the alloy. However, the *ab initio* calculations (figure 10) show that the population of electrons at the Fermi level is much smaller for S than for P or B, indicating a less metallic

environment (and therefore reduced screening conditions) for S in Ni–S. Although there is an overall Ni  $\rightarrow$  X (X = B, P, S) charge transfer, significant intra-atomic redistribution also takes place. This might be a serious factor influencing the inter-atomic bonding. It has been suggested [34] that the type of inter-atomic bonding and the bond strength can dominate AP shifts. Strong inter-atomic bonding (covalent type) associated with s–p–d hybridization may be the reason behind reduced AP values even though increased screening due to charge transfer would indicate the opposite. Formation of strong bonds due to s–p–d hybridization is accompanied by an increased d population on the Ni sites without formal electron transfer to the Ni sites. In the present study there are signs in the DOS of intra-atomic charge transfers for both Ni and the alloying addition sites. This is not surprising since in transition metals, d and non-d charge change (transfer) may occur in opposite directions, so the net charge change at a transition metal site tends to be opposite in sign to that of the d charge change [35, 36]. Moreover, hybridization of a transition metal atom's occupied states with the unoccupied levels of some other partner element atom is interpreted as a loss of the d weight in the occupied states and hence a loss of d count at the site [37]. It must be emphasized that the DFT calculations do not properly include the strong correlations that can be expected to arise between the initial and final state Ni 3d electrons; nevertheless, we believe that the overall picture which can be drawn from the calculations is correct.

As shown in figure 10, the lowest-lying valence bands in Ni and S (between  $-9$  and  $-6$  eV) are sp and, to a certain extent, spd hybridized. The main p band of S is at lower energy than those of P and B, indicating a stronger bonding and, therefore, less mobile screening electrons. There is no valence band below the lowest p band in Ni–S. Ni–B and Ni–P have Ni sp bands and P/B s bands at the lowest parts of the valence band ( $-14$  to  $-10$  eV). These bands are probably less localized than the spd bands between  $-9$  and  $-6$  eV. In covalent semiconductors the radial maximum of  $sp^3$  hybrid orbitals is greater than the inter-nuclei distance of adjacent sites and thus it is expected that delocalized screening may be important in these compounds. The more localized p states and the reduced presence of s states as compared to B and P could also lead to reduced core hole screening on the S sites in the Ni–S alloy. The above is in accord with the equivalent cores approximation in which a photoionized atom with atomic number  $Z$  can be considered equivalent to an atom with atomic number  $Z + 1$ . In the periodic table, phosphorus ( $3s^23p^3$ ) is followed by sulfur ( $3s^23p^4$ ) and S by Cl ( $3s^23p^5$ ). It is therefore more likely for a core hole in the P or S atom to be screened by a p valence electron than by an s electron. The hybridized bonds formed in the alloys may also be responsible for the reduced  $\alpha'$  values for Ni.

The use of the Bremsstrahlung radiation to acquire the P and S KLL peaks used to measure the P and S AP is beneficial in the following respect. The matrix element of an Auger process usually involves the wavefunction of a core orbital, and the Auger transition will only sample the local electronic structure [38]. Thus, the localized character of the final states of the Auger transition contrasts with the delocalized nature

of screening in semiconductors such as P and S; therefore it is difficult to distinguish contributions of the local and non-local DOS in Auger profiles of semiconductors involving the valence band [39]. By acquiring the Bremsstrahlung induced P and S KLL in the present study we probe only core levels and we overcome the above problem, probing thus only the P and S DOS.

#### 4. Conclusions

DFT was combined with XPS and XAES in an effort to gain insight into the alloying of Ni with B, S and P. It was shown that alloying of Ni with these elements is accompanied with an electron transfer from the Ni towards the alloying element sites but also an increase of the Ni 3d occupancy as a result of hybridization. This picture can explain to a good extent Auger parameter changes as well as the variation in the Ni 2p satellite.

#### Acknowledgments

This work resulted from the project ‘Nanocrystalline Alloys in Hydrogen Processes’ (project number 154258/431), funded by the Research Council of Norway. Provision of samples by T Knutsen, T Tønnessen and J Lerhman (Universitet i Agder, Norway) and provision of experimental facilities by Professor J F Watts (University of Surrey, UK), as well as fruitful discussions with Professor J Taftø (Universitet i Oslo), are gratefully acknowledged.

#### References

- [1] Lerhmann J, Burchardt T and Grøntoft T 2000 *Proc. 13th World Hydrogen Conf. (Beijing)* p 973
- [2] Våland T, Burchardt T and Grøntoft T 2002 *Int. J. Hydrog. Energy* **27** 39
- [3] Burchardt T 2000 *Int. J. Hydrog. Energy* **25** 627
- [4] Diplas S, Jørgensen S, Taftø J, Tønnessen T, Knutsen T, Lehrmann J, Våland T, Abel M-L and Watts J F 2006 *Surf. Interface Anal.* **38** 238
- [5] Yoshita S *et al* 1984 *J. Chem. Soc. Faraday Trans.* **80** 1435
- [6] Deng J F *et al* 1994 *Appl. Surf. Sci.* **81** 341
- [7] Xia W S, Fan Y and Jiang Y S 1996 *Appl. Surf. Sci.* **103** 1
- [8] Chen Y 1998 *Catal. Today* **44** 3
- [9] Li H *et al* 1999 *Appl. Surf. Sci.* **152** 25
- [10] Wagner C D, Gale L H and Raymond R H 1979 *Anal. Chem.* **51** 466
- [11] Moretti G 1998 *J. Electron Spectrosc. Relat. Phenom.* **95** 95
- [12] Kotani A and Toyozawa Y 1974 *J. Phys. Soc. Japan* **37** 912
- [13] Hüfner S 2003 *Photoelectron Spectroscopy, Principles and Applications* 3rd edn (Berlin: Springer)
- [14] Hillebrecht F U *et al* 1983 *Phys. Rev. B* **27** 2179
- [15] Diplas S, Lehrmann J, Jørgensen S, Våland T and Taftø J 2005 *Phil. Mag.* **85** 981
- [16] Castle J E and West R H 1979 *J. Electron Spectrosc. Relat. Phenom.* **16** 195
- [17] Castle J E and West R H 1980 *J. Electron Spectrosc. Relat. Phenom.* **18** 355
- [18] CasaXPS <http://www.casaxps.com>
- [19] Perdew J P, Burke K and Ernzerhof M 1996 *Phys. Rev. Lett.* **77** 3865
- [20] Kresse G and Furthmüller J 1996 *Phys. Rev. B* **54** 11169
- [21] Kresse G and Hafner J 1993 *Phys. Rev. B* **47** 558
- [22] Kresse G and Joubert D 1999 *Phys. Rev. B* **59** 1758
- [23] Blum P 1952 *J. Phys. Radium* **13** 430
- [24] Larsson E 1965 *Ark. Kem.* **23** 335
- [25] Gumeniuk R, Borrmann H and Leithe-Jasper A 2006 *Z. Kristallogr. New Cryst. Struct.* **221** 425
- [26] Rost E and Vestersj E 1968 *Acta Chem. Scand.* **22** 819
- [27] Massalski T B (ed) 1986 *Binary Alloy Phase Diagrams* vol 1 (Metals Park, OH: ASM)
- [28] Emsley J 1998 *The Elements* 3rd edn (Oxford: Clarendon)
- [29] Hume-Rothery W and Powell H M 1935 *Z. Kristallogr.* **91** 23
- [30] Hume-Rothery W 1969 *Atomic Theory for Students of Metallurgy* (London: The Institute of Metals)
- [31] Hume-Rothery W, Smallman R W and Haworth C W 1969 *The Structure of Metals and Alloys* (London: The Institute of Metals)
- [32] Matthew J A D *et al* 1995 *J. Phys. D: Appl. Phys.* **28** 1702
- [33] Gaarenstroom S W and Winograd N 1977 *J. Chem. Phys.* **67** 3500
- [34] Evans J A *et al* 1992 *Phys. Rev. B* **46** 1513
- [35] Kleiman G G and Landers R 1998 *J. Electron Spectrosc. Relat. Phenom.* **88** 435
- [36] Nørskov J K, Bligaard T, Logadottir A, Kitchin J R, Chen J G and Pandalov S 2005 *J. Electrochem. Soc.* **152** J23
- [37] Diplas S, Watts J F, Tsakirooulos P, Shao G, Beamson G and Matthew J A D 2001 *Surf. Interface Anal.* **31** 734
- [38] Friedman R M *et al* 1973 *Phys. Rev. B* **8** 2433
- [39] Gelatt C D and Ehrenreich H 1974 *Phys. Rev. B* **10** 398
- [40] Watson R E and Bennett L H 1978 *Phys. Rev. B* **18** 6439
- [41] Matthew J A D and Komninos Y 1975 *Surf. Sci.* **53** 716
- [42] Weightman P 1998 *J. Electron Spectrosc. Relat. Phenom.* **93** 165